IL NUOVO CIMENTO **46 C** (2023) 68
DOI 10.1393/ncc/i2023-23068-y

COMMUNICATIONS: SIF Congress 2022

Airborne EM in northern Italy for sustainable and resilient management of groundwater resources

N. A. L. SULLIVAN([1]) on behalf of M. GISOLO([2]), L. SPAGNOLI ([2]), A. RAPITI([3]), F. DAUTI([1])([3]), A. MENGHINI([3]), A. VIEZZOLI([3]) and G. FIANDACA([1])

([1]) *The EEM Team for Hydro & eXploration, Department of Earth Sciences Ardito Desio, University of Milan - Milan, Italy*

([2]) *A2A Ciclo Idrico S.p.A. - Brescia, Italy*

([3]) *EMergo S.r.l. - Cascina (PI), Italy*

received 11 April 2023

Summary. — Climate change and anthropogenic pollution pose a significant challenge to the management of groundwater resources in northern Italy, where in 2022 alone rainfall decreased by 40% compared to the average of the previous 30 years and 67% of the utilized agricultural area is vulnerable to nitrate pollution. To face these challenges, starting in the spring of 2021, A2A Ciclo Idrico initiated a large-scale Airborne electromagnetics (AEM) campaign for mapping the groundwater resources in the Brescia province, Italy, consisting of more than 2000 linear kilometers of AEM data flown over an area of approximately 200 km^2. This mapping campaign is the largest AEM campaign carried out in Italy for groundwater management, both in terms of extension and data density. Despite of the large anthropization of Brescia province, with the related problems of inductive couplings that disturb AEM data in the vicinity of buildings and infrastructures, excellent resistivity models have been retrieved in the flown areas, in a range of depths between 300 meters to 400 meters, thanks to careful data processing. This has allowed to map the groundwater resources with unprecedented coverage and resolution, both discovering new aquifers and highlighting their vulnerability. In particular, pathways for nitrate contamination in existing wells have been imaged, and the location for a new well for public water supply has been identified within an extended aquifer overlain by a clay layer that protects against pollution percolating from shallower aquifers. Moreover, 3D geological and hydrogeological models informed by AEM have been constructed in the valley of the Chiese river, and incorporated in a groundwater flow model of the area. These results triggered an even larger AEM campaign currently ongoing over all the plain and a mountainous sector of Brescia province, which we believe are the beginning of a paradigm shift in groundwater management in Italy towards resilient and sustainable exploitation of geo resources.

1. – Introduction

Northern Italy, where our study is focused, is characterized by a large alluvial valley bordered by the Alps to the North and West, by the Apennine chain to the South and by the Adriatic Sea to the East. The Po River basin, which hosts one of the largest multi-aquifer systems in Europe, is the most developed and densely inhabited area in Italy: the four largest regions of the area (Piemonte, Lombardia, Emilia Romagna and Veneto) account approximately for 30% of the surface, 40% of the population [1] and 50% of the Gross Domestic Product [2] of Italy. The Po Valley is also the most important agricultural and farming area in Italy, and water consumption for agriculture, industry and domestic use is among the highest in Europe [3]. However, in the last years the Po River basin has become vulnerable to drought, also as a consequence of climate change: in 2022 the highest average temperature since 1800 was reached, with + 1.28 degree compared to the average of the thirty years 1990–2020, as well as a decrease of 40% of precipitations [4]. Furthermore, the intensive agriculture and farming makes the Po Valley particularly vulnerable to nitrate pollution, with 67% of the utilized agricultural area identified as Nitrate Vulnerable Zone [5]. To face these challenges the in-depth knowledge of groundwater, as well as pathways of pollution migration, is essential. In this context, a large-scale Airborne Electromagnetic (AEM) campaign has been conducted in the Brescia province, aimed at the hydro-stratigraphic characterization of the basin, with focus on the individuation of aquifers, as well as preferential pathways of nitrate pollution.

AEM is a highly cost-effective method [6] that allows to map the 3D distribution of electrical resistivity measuring while flying, with an unmatched efficiency in imaging large areas in short acquisition times, and allowing a spatial coverage of the subsoil and depths of investigation not reached by boreholes. Large-scale AEM surveys are increasingly used for studying groundwater resources, with recent applications for instance in the central valley of California [7] and the Mississippi valley [8]. Regarding AEM surveys in Italy, a few campaigns were carried out in the last decade: the Venice lagoon was partially surveyed in 2010 and in 2013, to map the freshwater aquifer under the lagoon and study the continental-marine superficial water-groundwater exchanges [9, 10]; AEM for geothermal exploration was conducted in Sicily in 2011 [11]; a first attempt of AEM for groundwater management was carried out in 2018 in the Milano Province (unpublished results).

The Brescia survey presented in this paper constitutes the first large-scale airborne campaign in Italy for aquifer characterization focused on a better groundwater management. In the following, after presenting the AEM methodology, we describe the survey campaign and the main results, in terms of resistivity models and their interpretation for withdrawal management and modelling of groundwater flow.

2. – Methodology

2˙1. *AEM method & forward modelling.* – The Airborne Time-Domain Electromagnetic (AEM) method is used to obtain the 3D resistivity model of the subsurface through the continuous measurements of the secondary electromagnetic field generated by the subsoil in response to the fast turn-off of a primary field in the transmitter carried by an airplane or a helicopter (fig. 1). In particular, the measurement procedure comprises the following steps: i) a continuous current is established in the transmitter loop, which generates the primary magnetic field; ii) the current is quickly turned off, and consequently the primary field as well, so that an electromotive force (emf) is induced in the subsoil, according to Faraday's law of induction; iii) the emf generates eddy currents in the sub-

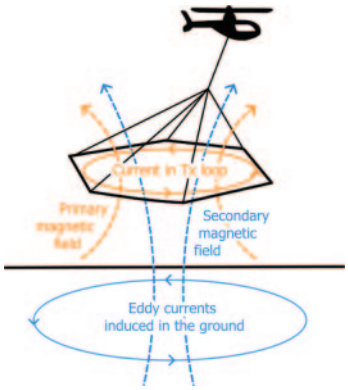

Fig. 1. – Functioning scheme of a helicopter-towed EM system. The current that flows in the transmitter (Tx) loop (orange continuous line) generates a primary magnetic field (dashed orange lines). After the turn-off of the current in the transmitter, the variation of the primary field induces eddy currents in the ground (continuous blue line), which generate the secondary field (dashed blue lines) measured in the receiver.

soil, which produce a secondary electromagnetic field measured by the receiver; iv) the eddy currents dissipate quickly through ohmic losses, with the corresponding secondary field decaying in function of the 3D resistivity distribution. All this measurement process takes up to a few tens of milliseconds, with the secondary field measured in the off-time after the current turn off; this allows to measure with a typical repetition frequency of 25Hz, with acquisition speed up to approximately 90 km/h. After acquisition, data are stacked in soundings, which are modeled with the assumption that physical parameters of sediments and rocks vary only with depth (1D modeling).

The 1D computation of the forward response $\frac{\partial B_{z,TD}(t)}{\partial t}$ at the receiver is carried out taking into account the filter characteristics of the receiver, the shape of the transmitter as well as the waveform of the current turn-off. Following Ward and Hohmann [12], this is achieved computing the forward response in frequency domain (FD) as superposition of horizontal electric dipoles along the transmitter loop as

$$B_{z,FD}(\boldsymbol{\sigma}, \mathbf{h}, \omega, x, y, z) = \oint_{Tx\,loop} \mathrm{d}B_{z,FD}, \tag{1}$$

where $\boldsymbol{\sigma} = \{\sigma_1, \dots, \sigma_N\}$ and $\mathbf{h} = \{h_1, \dots, h_{N-1}\}$ represent the electric conductivity and the layer thicknesses of a N-layered 1D model, ω is the angular frequency, x, y, z indicate the position of the receiver and $\mathrm{d}B_{z,FD}$ is the contribution of the infinitesimal loop piece of length ds, expressed as

$$\mathrm{d}B_{z,FD}(\boldsymbol{\sigma}, \mathbf{h}, \omega, x_*, y_*, z_*) = \frac{I\mathrm{d}s}{4\pi} \cdot \frac{y_*}{\rho_*} \int_0^\infty (1 + r_{TE}) e^{u_0 z_*} \frac{\lambda^2}{u_0} J_1(\lambda \rho_*) \mathrm{d}\lambda \tag{2}$$

where x_*, y_*, z_* are the receiver coordinates in the reference system that sees the infinitesimal loop piece $\mathrm{d}s$ oriented in the x direction and centered at its origin, J_1 represents the Bessel function of order 1, $\rho_* = \sqrt{x_*^2 + y_*^2}$ is the distance between the receiver and the segment origin, I is the current in the loop, $u_0 = \sqrt{\lambda^2 - \omega^2 \mu_0 \epsilon_0}$ and r_{TE} represents

the reflection coefficient of the electric field transverse to the z-axis, defined as

$$r_{TE} = \frac{Y_0 - \hat{Y}_1}{Y_0 + \hat{Y}_1} \tag{3}$$

where the intrinsic admittance of the free space Y_0 and the surface admittance $\hat{Y}_1$ are computed using the relations

$$\hat{Y}_n = Y_n \frac{\hat{Y}_{n+1} + Y_n \cdot \tanh(u_n h_n)}{Y_n + \hat{Y}_{n+1} \cdot \tanh(u_n h_n)}, \tag{4a}$$

$$Y_n = \frac{u_n}{\hat{z}_n}, \tag{4b}$$

$$\hat{y}_n = \sigma_n + i\epsilon_n\omega, \tag{4c}$$

$$\hat{z}_n = i\mu_n\omega, \tag{4d}$$

$$u_n = \sqrt{\lambda^2 - k_n^2}, \tag{4e}$$

$$k_n^2 = -\hat{y_n}\hat{z}_n, \tag{4f}$$

$$\hat{Y}_N = Y_N, \tag{4g}$$

where the computation of $\hat{Y}_1$ is performed iteratively, starting from the last layer N. In all equations no variations in dielectric permittivity and magnetic permeability are assumed among layers (*i.e.*, $\epsilon_n = \epsilon_0$ and $\mu_n = \mu_0$).

The integral of eq. (2) is computed through fast Hankel transforms following Johansen and Sørensen [13].

The time-domain (TD) step response $B_{z,TD,step}$ is then computed through a cosine transform of the imaginary part of FD kernel, while the impulse response though sine transform of the real part of the kernels, as

$$B_{z,TD,step}(\boldsymbol{\sigma}, \mathbf{h}, t, x, y, z) = \frac{2}{\pi} \int_0^\infty \frac{\Im(B_{z,FD}(\boldsymbol{\sigma}, \mathbf{h}, \omega, x, y, z) \cdot F(\omega))}{\omega} \cos(\omega t) \mathrm{d}\omega, \tag{5a}$$

$$B_{z,TD,impulse}(\boldsymbol{\sigma}, \mathbf{h}, t, x, y, z) = \frac{2}{\pi} \int_0^\infty \Re(B_{z,FD}(\boldsymbol{\sigma}, \mathbf{h}, \omega, x, y, z) \cdot F(\omega)) \sin(\omega t) \mathrm{d}\omega, \tag{5b}$$

where $F(\omega)$ represents the FD filter characteristics of the receiver. Also the cosine/sine transforms are solved numerically in terms of Hankel transforms, expressed in terms of Bessel functions of order -1/2 and +1/2, respectively [13]:

$$\frac{1}{\pi} \int_0^\infty f(\omega)^{\cos}_{\sin}(\omega t) \mathrm{d}\omega = \sqrt{r} \int_0^\infty f_1(\lambda) \lambda J_{\pm 1/2}(\lambda r) \mathrm{d}\lambda, \tag{6}$$

where $r = t\sqrt{2\pi}, \lambda = \frac{\omega}{\sqrt{2\pi}}$ and $f_1(\lambda) = \frac{1}{\sqrt{\lambda}} f\left(\frac{\lambda}{\sqrt{2\pi}}\right)$.

Finally, the time-derivative $\frac{\partial B_{z,TD}(t)}{\partial t}$ of the magnetic field measured at the receiver is computed as the time-derivative of the convolution of the impulse response with the

current waveform $i(t)$ in the transmitter:

$$\frac{\partial B_{z,TD}(t)}{\partial t} = \frac{\partial (B_{z,TD,impulse}(t) * i(t))}{\partial t} = B_{z,TD,impulse}(t) * \frac{\partial i(t)}{\partial t}, \tag{7}$$

where the second equality makes use of the rules of the derivative of convolutions. Equation (7) is solved as proposed by Fitterman and Anderson (1986) [14] for piecewise linear current waveforms:

$$\frac{\partial B_{z,TD}(t)}{\partial t} = \sum_{j=1}^{M} \Delta i_j \cdot \frac{B_{z,TD,step}(t - t_j + \Delta t_j) - B_{z,TD,step}(t - t_j)}{\Delta t_j}, \tag{8}$$

where the summation is carried over all the M piecewise linear segments of the current $i(t)$ defined in the time intervals $\{t_j, t_j + \Delta_j\}$ with slopes $\Delta i_j / \Delta t_j$.

2˙2. *Acquisition and processing.* – The system used for the survey is a SkyTEM 312 helicopter-towed time-domain system, in which the transmitter loop is mounted on a hexagonal frame of $342\,\mathrm{m}^2$ of area and the receiver loop is mounted on one end of the frame, in a position in which the primary field is null. The SkyTEM 312 system uses two energizing magnetic moments: a low moment ($\approx 4600\,\mathrm{Am}^2$) that allows a fast turn off ($13\,\mu$s) to retrieve information about the near surface and a high moment ($\approx 430.000\,\mathrm{Am}^2$) with slower turn off ($300\,\mu$s) but greater depth of penetration. The typical flight speed in the survey ranged within (70 to 90) km/h, with an altitude of (30 to 35) m above the ground. Before inversion, an accurate processing of the data is necessary, to remove the data where the signal is affected by inductive coupling with man-made infrastructures. The data processing has been carried out in two phases: i) in quasi real-time during the acquisition period, to adapt the acquisition plan to the results as they were produced; ii) after the survey completion, with careful removal of all interferences.

2˙3. *Inversion.* – The data were inverted using the spatially constrained inversion (SCI) presented in Viezzoli *et al.* [15], through a linearized iterative approach. The model vector $\mathbf{m}_n$ of the n-th iteration of the inversion comprises the resistivity values (the inverse of the conductivities used for the forward response) of the N-layers 1D models (30 layers with log-increasing depths from 4 m to 400 m in the current application) of all the soundings of the survey, while the data vector $\mathbf{d}$ is formed by the measured $\frac{\partial B_{z,TD}(t)}{\partial t}$ values of all soundings not removed in the processing phase. Vertical constraints are imposed between resistivity values of consecutive layers in each 1D model and lateral constraints are imposed among corresponding layers of neighbour models. A uniform relative strength has been used for the vertical constraints, while the strength of the horizontal constraint is scaled with the distance between 1D models. The model update at the $(n+1)$-th iteration is computed with the Levenberg-Marquardt approach as [16]

$$\mathbf{m}_{n+1} = \mathbf{m}_n + [\mathbf{G}^T \mathbf{C}_d^{-1} \mathbf{G} + \mathbf{R}^T \mathbf{C}_R^{-1} \mathbf{R} + \lambda \mathbf{I}]^{-1} \cdot [\mathbf{G}^T \mathbf{C}_d^{-1} (\mathbf{d} - \mathbf{f}(\mathbf{m}_n)) + \mathbf{R}^T \mathbf{C}_R^{-1} \mathbf{R} \mathbf{m}_n] \tag{9}$$

where $\mathbf{G}$ represents the Jacobian of the n-th iteration, $\mathbf{R}$ is the roughness matrix containing the information on the constrained parameters [16], $\mathbf{f}(\mathbf{m}_n)$ is the forward response computed through eqs. (1)–(8), $\lambda \mathbf{I}$ represents the damping [16] and $\mathbf{C}_d$ and $\mathbf{C}_R$ are the covariance matrices [16] of the data and roughness constraints, respectively.

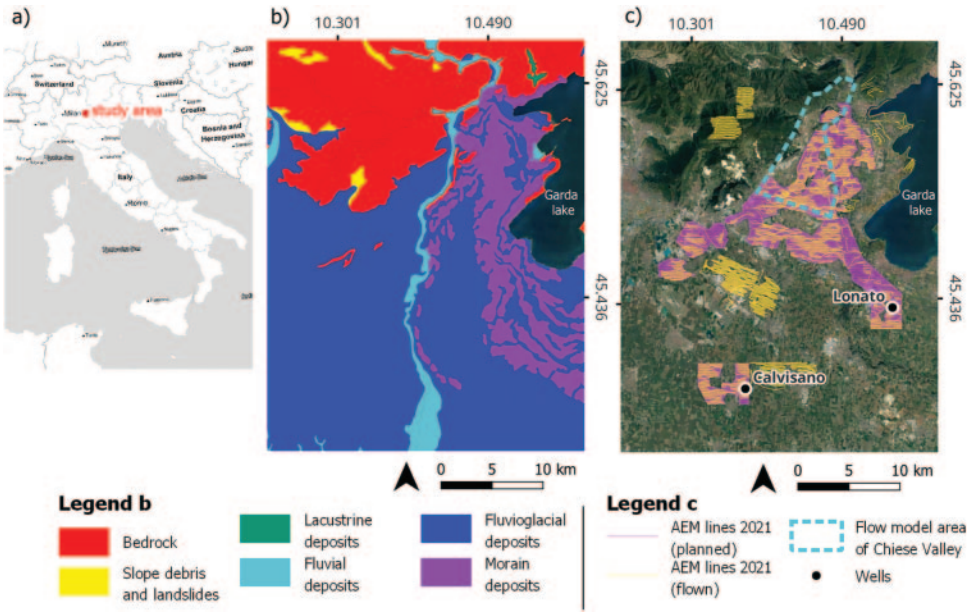

Fig. 2. – Study area: (a) map of Italy and location of the Brescia province marked with the red dot; (b) geological map of the lithologies from Geologic Map of Lombardy at 1:250.000 scale [19]; (c) planned flight lines (purple area) and flown lines (yellow lines), area of groundwater flow model (dashed light blue line) and location of wells (black dots) presented in this study.

3. – The Brescia survey

3˙1. *Survey layout and site description.* – The Brescia survey has been carried out on an area of approximately 200 km^2 on the west shore of the Garda Lake (fig. 2) and was commissioned by A2A Ciclo Idrico S.p.A., one of the two water management companies operating in Brescia province, under the supervision of the ATO Brescia, the local authority that regulates and supervises the public supply of water.

The geology of the flown area is mainly composed by fluvioglacial, moraine and fluvial deposits, with outcropping bedrock in the northwestern portion (fig. 2(b)). The glacial deposits that are present in the area belong to the Garda morainic amphitheater. These deposits have strong variability both horizontally and vertically, including erosive gaps, due to the advance and retreat of the glacier during the different glacial periods to which the area has been subject. The alluvial deposits constitute the alluvial plain of Chiese river and river terraces of old floods [17].

The flight lines were designed by excluding urban areas and coupling elements like electrified or metal structures and roads. The plan was revised daily accordingly to the preliminary inversion results given day by day by the company in charge of data interpretation (Emergo s.r.l.), in order to cover adequately the geological structures identified by AEM. Figure 2(c) presents all the final flight lines. At the end of February 2021 about 2.000 linear km were flown in less than two weeks, retrieving 60.000 individual surveys (and models) with a density of 200 models/km^2, with spacing between flight lines of approximately 75 m. This high data density after processing proves that also in a highly urbanized area like Brescia province the AEM surveying has unmatched mapping capabilities.

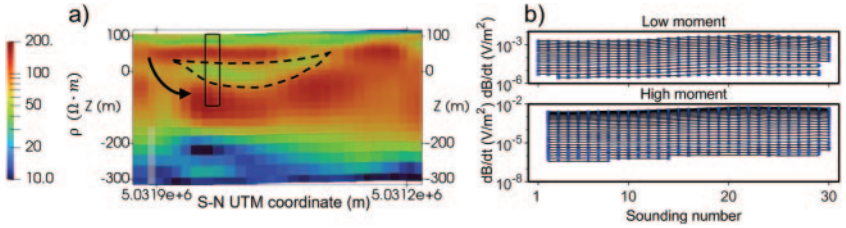

Fig. 3. – Lonato case study. (a) Resistivity NS profile closest to the well. The well is shown with a black rectangle, the clay layer above the well screen by dashed lines and the pathway of contamination by the arrow. Shaded areas are below the depth of investigation [18]. (b) Corresponding sounding-by-sounding $\mathrm{d}B/\mathrm{d}t$ data (blue markers) and gate-by-gate data fit (continuous black lines).

3˙2. *Results: withdrawal management.* – The results of the AEM campaign have been used for the management of existing wells and the planning of new drillings. The first case presented in this study regards aquifer contamination by nitrates in the area of Lonato (Brescia), in the south-east of the study area (fig. 2(c)). A new well for drinking water was established in 1997. Considering that the area presented significant levels of nitrate pollution in the shallow aquifers, the well location was identified in a zone where boreholes evidenced a continuous clay layer acting as a barrier to the percolation of nitrates. Unfortunately, after a few years of exercise, nitrates pollution appeared in Lonato's new well. Figure 3 shows the AEM resistivity model (a) of the line closest to the well, together with the corresponding data and fit (b). In the resistivity section (a), the more resistive parts (orange to brown) are the groundwater bearing formations, while the more conducive areas (blue to green) are the clay layers that confine the aquifer, with depth of investigation [18] down to 400 m. The clay layer that separates the shallower and the deeper aquifers, identified by the boreholes when the well was planned, is only a local protection: hydraulic communication between the shallower and deeper aquifer (pathways for nitrate percolation to the deep aquifer) unidentified by boreholes are clearly evident in the AEM inversion, as indicated by the arrow in fig. 3(a). This result highlights the importance of the areal coverage of the AEM data not only in the characterization of groundwater resources, but also in the evaluation of the contamination risk.

The mapping capabilities of the AEM campaign have been used for the identification of the area for a new well for public supply in the Calvisano municipality (fig. 2(c)), the second case presented in this study. In 2020 a first drilling was carried out down to 147 m, based on scarce borehole information (there are hundreds of wells in the area, but none of them deeper than 40 m), but unfortunately only basal clays were encountered in the perforation, at a shallower depth than expected. Also in this case, the interpretation of the AEM results provides new subsurface data in sedimentary areas characterized by low-energy deposits, mapping the high-permeability areas (resistive areas interpreted as saturated sand and gravel formations), *i.e.*, new aquifers. Based on the AEM evidence, a new location for a drilling was identified based on two characteristics (fig. 4): i) high resistivity at the depth of interest, continuous in the north direction, indicating a sustainable recharge from the high plains; ii) continuous coverage of the deep aquifer by a continuous clay layer, which protects the deep aquifer from anthropogenic pollution. The authorization procedure for the new well is ongoing, with drilling planned in 2023.

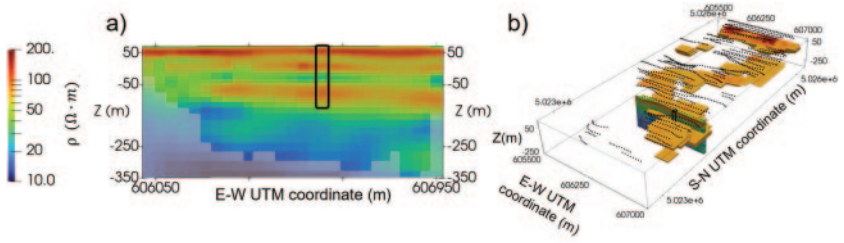

Fig. 4. – Calvisano case study. a) Resistivity model in correspondence to the identified location for the new well. Black rectangle: planned well. Shaded areas are below the depth of investigation [18]. b) Volume of high resistivity (greater than 80 Ω m) below −50 m in elevation imaged by AEM, extending to the north of the area. Black rectangle: planned well; black dots: AEM soundings.

3˙3. *Results: 3D geological & hydrogeological modelling*. – The AEM resistivity models were also used to build a 3D geological and hydrogeological model of the basin of the middle Chiese River, whose area is delimited in fig. 2(c). The geological model was built using a cognitive approach [20], presented in fig. 5: interface surfaces between different geological units are identified in the geophysical sections based on resistivity contrast and borehole information, and used to delineate geological units in 3D. The 3D geological model was then used to build a finite-element 3D groundwater flow model in FeFlow [21], informed by measurements of hydraulic head in 29 boreholes measured in 4 piezometric campaigns between 2021 and 2022. In particular, the AEM results helped in setting properly the boundary conditions of the model in the north area, where the bedrock acts as an aquitard and in the eastern zone where the hydrogeological boundary between alluvial and glacial deposits has been identified.

3˙4. *Outlook*. – The success of the 2021 AEM campaign triggered an even larger AEM campaign, planned and managed by A2A Ciclo Idrico S.p.A. and Acque Bresciane under the supervision of ATO Brescia: by summer 2023 AEM data will be acquired in the entire province of Brescia over approximately 20000 linear kilometers (fig. 6). Furthermore, the HydroGeosITe, the first Italian reference and calibration site for AEM and ground electric and electromagnetic surveys for hydrogeological applications is being established in Bedizzole (BS), for helping the interpretation of AEM models and ensuring the quality

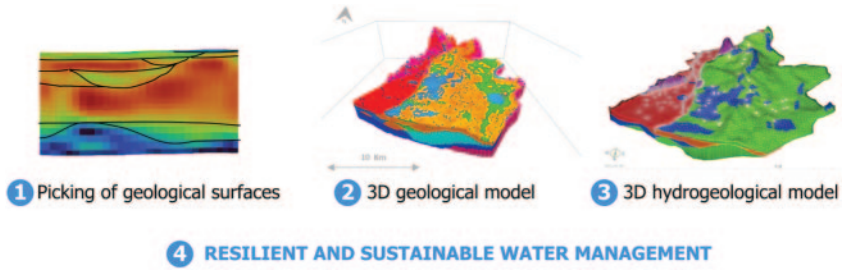

Fig. 5. – AEM-based workflow of water management: 1) picking of interface surfaces between geological units based on AEM models and borehole information; 2) construction of 3D geological model based on the identified interface surfaces; 3) groundwater flow modelling based on the 3D geological model; 4) resilient and sustainable water management based on AEM-informed groundwater flow modelling.

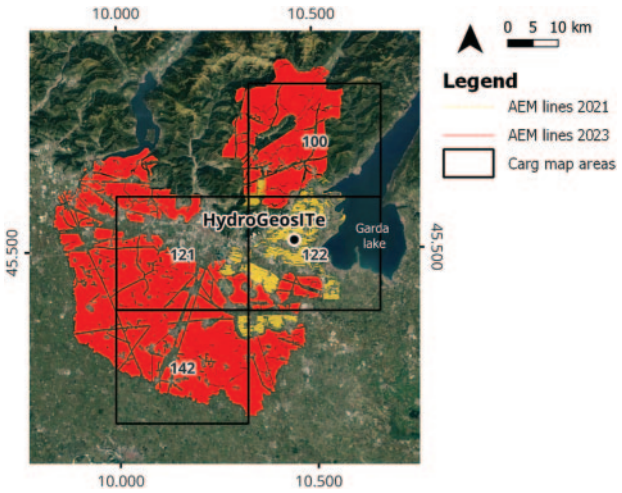

Fig. 6. – Flight lines of the AEM survey of 2021 (yellow) and plan of the ongoing 2023 campaign (red), together with the areas of the 1:50.000 CARG geological sheets covered for more than 50% by AEM data.

of geophysical data. This survey will add invaluable information to approach the design of interventions on public aqueducts with greater awareness (for instance new wells, aqueduct interconnections and artificial groundwater recharge), allowing the decision makers to establish sustainable solutions based on knowledge and, more in general, a modern management of resources. These solutions may include, for example: tailoring the groundwater withdrawal on the actual recharge, evaluated also through groundwater modelling; engineering groundwater recharge in suitable areas identified by AEM; explore deep groundwater resources, not mapped in details by boreholes but imaged in the AEM models. The knowledge acquired with these AEM campaigns is not restricted only to groundwater, but will benefit all the areas linked to the subsoil, such as: the geological mapping, the risk assessment, the geotechnical engineering and in general the exploitation of geo resources.

As an example of the potential of the AEM surveying outside the specific aim of the Brescia campaigns, focused on groundwater characterization, in fig. 6 the AEM survey lines are superposed with the boundaries of the four CARG geological sheets (*i.e.*, the official 1:50.000 New Italian geological maps) covered by AEM data for more than 50% of their extension. None of these four sheets is already completed: the compilation of sheet 121 (Brescia sheet) is ongoing, but sheet 100 (Salò), sheet 122 (Desenzano del Garda) and sheet 142 (Manerbio) have not been assigned yet for execution. We believe that the AEM surveys in Brescia province will make a key contribution to the new geological maps of those sheets.

4. – Conclusions

We presented the results of the largest AEM campaign carried out in Italy focused on aquifer characterization and groundwater management. AEM results have proven to be an invaluable tool for understanding the heterogeneity of alluvial granular deposits with an obvious positive effect in groundwater management. AEM helps in identifying the best site for drilling new wells, mapping the extent and lateral continuity of aquifer

formations, as well as the vulnerability of captured aquifer to various anthropogenic contaminations, thanks to its ability to image the lateral extent of the clayey aquifer cover, a natural barrier to contamination. In addition, the integration of AEM models and complementary traditional stratigraphic information derived from boreholes allows to build new basin-scale geological and hydrogeological models that preserve the complexity of the structures of different depositional environments. This allows the construction of highly plausible groundwater flow models, which are essential for modern groundwater management. The excellent results of the 2021 AEM campaign triggered a second AEM campaign, ongoing in 2023, which covers the entire plain of Brescia province and a mountainous sector. We believe that these surveys are the beginning of a paradigm shift in the groundwater management in Italy, which will allow to face the challenges posed by climate change and to build a resilient and sustainable management of geo resources.

* * *

This work has been carried out within the projects CE4WE, funded by Lombardia Region and HydroEEMaging - Electric and Electromagnetic imaging of Hydro resources, funded by A2A Ciclo Idrico S.p.A.

REFERENCES

[1] ISTAT, *Censimenti permanenti* (2022) URL: `http://dati-censimentipermanenti.istat.it/?lang=it`.
[2] ISTAT, *Prodotto interno lordo lato produzione* (2022) URL: `http://dati.istat.it/Index.aspx?`.
[3] ISTAT, *Water report* (2019) URL: `https://www.istat.it/it/files//2019/03/Water-report.pdf`.
[4] CNR, *Climate monitoring for Italy* (2023) URL: `https://www.isac.cnr.it/climstor`.
[5] ISTAT, *6th general census of agriculture* (2010) URL: `http://dati-censimentoagricoltura.istat.it/Index.aspx`.
[6] Siemon B., Christiansen A. V. and Auken E., *Near Surf. Geophys.*, **7** (2009) 629.
[7] Knight R., Smith R., Asch T., Abraham J., Cannia J., Viezzoli A. and Fogg G., *Groundwater*, **56** (2018) 893.
[8] Minsley B. J., Rigby J. R., James S. R., Burton B. L., Knierim K. J., Pace M. D., Bedrosian P. A. and Kress W. H., *Commun. Earth Environ.*, **2** (2021) 131.
[9] Viezzoli A., Tosi L., Teatini P. and Silvestri S., *Geophys. Res. Lett.*, **37** (2010) L01402.
[10] Tosi L., Da Lio C., Teatini P., Menghini A. and Viezzoli A., *Proc. Int. Assoc. Hydrol. Sci.*, **379** (2018) 387.
[11] Santilano A., Manzella A., Donato A., Montanari D., Gola G., Di Sipio E., Destro E., Giaretta A., Galgaro A., Teza G. *et al.*, *Shallow geothermal exploration by means of skytem electrical resistivity data: an application in Sicily (Italy)*, in Proceedings of *Engineering Geology for Society and Territory*, Vol. **1**: *Climate Change and Engineering Geology* (Springer) 2015, pp. 363–367.
[12] Ward S. H. and Hohmann G. W., *Electromagnetic theory for geophysical applications*, in *Electromagnetic Methods in Applied Geophysics*, Vol. **1**, *Theory* (Society of Exploration Geophysicists) 1988, pp. 130–311.
[13] Johansen H. and Sørensen K., *Geophys. Prospect.*, **27** (1979) 876.
[14] Fitterman D. V. and Anderson W. L., *Geoexploration*, **24** (1987) 131.
[15] Viezzoli A., Christiansen A. V., Auken E. and Sørensen K., *Geophysics*, **73** (2008) F105.

[16] Auken E., Christiansen A. V., Kirkegaard C., Fiandaca G., Schamper C., Behroozmand A. A., Binley A., Nielsen E., Effersø F., Christensen N. B. *et al.*, *Explor. Geophys.*, **46** (2015) 223.
[17] Conti M. and Conti A., Tech. Rep. Comune di Bedizzole (Comune di Bedizzole) (2009).
[18] Christiansen A. V. and Auken E., *Geophysics*, **77** (2012) WB171.
[19] Regione-Lombardia, *Carta geologica 250.000* (1990) URL: `https://www.geoportale.regione.lombardia.it`.
[20] Jørgensen F., Møller R. R., Nebel L., Jensen N.-P., Christiansen A. V. and Sandersen P. B., *Bull. Eng. Geol. Environ.*, **72** (2013) 421.
[21] Trefry M. G. and Muffels C., *Groundwater*, **45** (2007) 525.